Ultrafast Excitonic Response in Two-Dimensional Hybrid Perovskites Driven by Intense Midinfrared Pulses

Shunran Li, Xiaotong Li, Conrad A. Kocoj, Xiaoqin Ji, Shaofan Yuan, Eleni C. Macropulos, Constantinos C. Stoumpos, Fengnian Xia, Lingling Mao, Mercouri G. Kanatzidis, and Peijun Guo

Phys. Rev. Lett. **129**, 177401 — Published 21 October 2022

DOI: 10.1103/PhysRevLett.129.177401

Ultrafast excitonic response in two-dimensional hybrid perovskites driven by intense mid-infrared pulses

Shunran Li[1,2], *Xiaotong Li*[3], *Conrad A. Kocoj*[1,2], *Xiaoqin Ji*[4], *Shaofan Yuan*[5], *Eleni C. Macropulos*[6], *Constantinos C. Stoumpos*[6], *Fengnian Xia*[5], *Lingling Mao*[4], *Mercouri G. Kanatzidis*[3], *Peijun Guo*[1,2,*]

[1]Department of Chemical and Environmental Engineering, Yale University, 9 Hillhouse Avenue, New Haven, CT 06520

[2]Energy Sciences Institute, Yale University, 810 West Campus Drive, West Haven, CT 06516

[3]Department of Chemistry, Northwestern University, 2145 Sheridan Road, Evanston, IL 60208

[4]Department of Chemistry, Southern University of Science and Technology, Shenzhen, China

[5]Department of Electrical Engineering, Yale University, 15 Prospect Street, New Haven, CT 06511

[6]Department of Materials Science and Technology, University of Crete, Voutes Campus, Heraklion 70013, Greece

*Email: peijun.guo@yale.edu

Abstract

Two-dimensional organic-inorganic hybrid perovskites (2DHPs) are natural quantum-well-like materials, in which strong quantum and dielectric confinement effects due to the organic spacers give rise to tightly bound excitons with large binding energy. To examine the mutual interactions between the organic spacer cations and the inorganic charge-residing octahedral framework in 2DHPs, here we perform femtosecond pump-probe spectroscopy by direct vibrational pumping of the organic spacers, followed by a visible-to-ultraviolet probe covering their excitonic resonances. Measurements on prototypical lead-bromide based 2DHP compounds, $(BA)_2PbBr_4$ and $(BA)_2(FA)Pb_2Br_7$ (BA=butylammonium; FA=formamidinium), reveal two distinct regimes of the temporal response. The first regime is dominated by a pump-induced transient expansion of the organic spacer layers that reduces the exciton oscillator strength, whereas the second regime arises from pump-induced lattice heating effects primarily associated with a spectral shift of the exciton energy. In addition, vibrational excitation enhances the biexciton emission, which we attribute to a stronger intralayer exciton confinement as well as vibrationally induced exciton detrapping from defect states. Our study provides fundamental insights regarding the impact of organic spacers on excitons in 2DHPs, as well as the excited-state dynamics and vibrational energy dissipation in these structurally diverse materials.

Keywords

Two-dimensional materials, organic-inorganic hybrid perovskites, pump-probe spectroscopy, mid-infrared, excitons, ultrafast spectroscopy

Two-dimensional organic-inorganic hybrid perovskites (2DHPs) are solution-processable semiconducting materials with remarkable light-absorbing and luminescent properties [1]. Compared to their three-dimensional (3D) counterparts which have risen as appealing light absorbers for photovoltaics [2], 2DHPs exhibit dramatically enhanced compositional and structural diversity. By incorporating various organic spacer cations between the octahedral layers, phases including the Ruddlesden-Popper and Dion-Jacobson phases can be formed [3-5] with different thicknesses and compositions [6,7]. Such chemical and structural diversity has enabled a variety of functionalities including improved stability [8], white-light emission [9], light emission and detection [10], and lasing [11]. Recently, 2DHPs exhibiting ferroelectricity, ferromagnetism, spin-selectivity and lateral heterojunctions have also emerged [12-15].

The charge-insulating and low-permittivity organic spacers impart both quantum and dielectric confinements on charge carriers, making 2DHPs strong excitonic materials with large exciton binding energies on par with 2D transition-metal dichalcogenides [16-18]. In addition to an impact on the exciton binding energy, organic spacers also strongly influence the phase-transition behavior, electronic bandgap, exciton self-trapping, and interlayer charge-carrier interactions [9,19,20]. Previous efforts focused on the examination of the optical [18], electronic [21], thermal [22], magnetic [23] and structural properties [24] of 2DHPs incorporating different inorganic and organic sublattices. Here, using time-resolved optical pump-probe spectroscopy, we investigate the interplay between the organic and inorganic sub-lattices in prototypical lead bromide (Pb-Br)-based 2DHPs [25]. Intense femtosecond (fs) mid-infrared (MIR) laser pulses are employed to impulsively stimulate the vibrations of the organic spacers, followed by probe pulses in the ultraviolet (UV)-to-blue range to distill the exciton dynamics. We observe two distinct temporal regimes: the first is dominated by a transient expansion of organic cations with the inorganic layers largely unaffected, whereas the second regime corresponds to MIR-pump induced lattice temperature rise. These experiments employing a vibrational pump and an electronic probe reveal the fundamental timescales of vibrational energy transfer between the two sublattices and the influence of organic spacers on the exciton oscillator strength in 2DHPs.

The 2DHPs investigated here have compositions of $(BA)_2PbBr_4$ and $(BA)_2(FA)Pb_2Br_7$, which are denoted as n=1 and n=2, respectively. Here, n corresponds to the number of octahedral layers per repeating unit, BA^+ is butylammonium or $CH_3(CH_2)_3NH_3^+$, and FA^+ is formamidinium or $(NH_2)CH(NH_2)^+$. The reported crystal structures [12,26] are displayed in Fig. 1a. These

structurally anisotropic 2DHPs, with nearly identical in-plane lattice constants along the *a* and *b* directions, can be approximated as uniaxial optical media with optic axis pointing along the *c* direction. The single-crystal flakes have mm lateral dimensions and tens-of-μm thicknesses, and measurements were performed on the *a*-*b* planes at normal or near-normal (<5°) incidences. Fig. 1b-1c present the steady-state reflectance over the spectral ranges of their excitonic resonances, measured at 78~295 K (Fig. S1). For both materials, the reflectance exhibits a minimum (maximum) on the blue (red) side of their exciton resonance [27]. Near the exciton resonances, the material's relative permittivity $\varepsilon(\omega)$ can be described by the Lorentzian oscillator model [28], $\varepsilon(\omega) = \varepsilon_\infty + \frac{{A_\mathrm{L}}^2}{{\omega_\mathrm{L}}^2-\omega^2-i\omega\gamma}$, where ε_∞, ω_L, γ, and A_L are the high-frequency relative permittivity, exciton resonance frequency, exciton damping factor, and exciton oscillator strength, respectively. Using the transfer-matrix method, we fit the four Lorentzian-model parameters (Table S1-S2) from the reflectance (Fig. S2). The spectral region in the fitting is confined to be above the absorption-onset wavelength. As demonstrated in Fig. S3, the absorption onset wavelength is located slightly to the red of the reflectance maximum; on the blue side of the absorption onset wavelength, the materials can be considered as infinitely optically thick media and their reflectance is only dependent on $\varepsilon(\omega)$ but not on material thickness. From the Lorentzian parameters, we find the two compounds have similar γ, but *n*=2 has a smaller A_L compared to *n*=1, consistent with previous observations of lead-iodide-based 2DHPs [17,29,30]. In addition, the exciton resonance in *n*=2 is redshifted than *n*=1, which arises from the layer thickness-dependent confinement effect that influences both exciton binding energy and material bandgap [30-33].

While the electronic transitions on the Pb-Br network manifest in the UV-to-blue range, the vibrational modes of the organic cations lie in the MIR range (Fig. S4) [34], including the N-H and C-H stretching vibrations (~3 μm). To examine the mutual interactions between the two sub-lattices, we perform pump-probe transient reflection experiments, where we selectively excite the N-H and C-H vibrational modes of the organic spacer cations using resonant MIR pump (3.0~3.2 μm) and probe the exciton resonances in the UV-to-blue range. Fig. 2a presents the transient spectral map of $\Delta R/R$ for *n*=1 at 78 K, where $\Delta R/R = [R(t) - R(0)]/R(0)$ with $R(0)$ being the reflectance without pump excitation and $R(t)$ the reflectance at delay time t after pump excitation. Fig. 2a demonstrates that the transient response at early time (<40 ps) is markedly different from that at later times (>40 ps). Such a difference manifests not only in the signal amplitude, but

notably in the spectral line-shape and even in the sign of the transient signal. To illustrate this difference more clearly, two transient spectra, representative of early and late delay times, are plotted in Fig. 2b. the 100-ps $\Delta R/R$ spectrum develops a positive lobe centered at 395 nm, surrounded by two asymmetric, negative lobes. In contrast, the 5-ps $\Delta R/R$ spectrum has a derivative-like line-shape, switching from positive to negative at about 392 nm. Similarly, two disparate regimes in the transient optical response are also observed for n=2 (Fig. 2c), whose representative transient $\Delta R/R$ spectra at early and late delay times (Fig. 2d) are consistent with n=1. Temperature-dependent measurements on both compounds yield similar timescales over 78~295 K, although the $\Delta R/R$ kinetics grows slightly faster at higher temperature (Fig. S5).

We first attempt to understand the late-time transient response by calculating $\Delta R/R$ using the steady-state, temperature-dependent reflectance data (Fig. 1b-1c). The results (Fig. S6) match the transient $\Delta R/R$ analogue and indicate that the late-time response is of thermal origin. Following vibrational excitation of the organic cations, phonon-phonon interactions between the organic and inorganic components take place during the first tens of ps. A thermal equilibrium between the two sublattices is established at 50~100 ps, after which the material occupies a higher temperature than that prior to pump excitation, producing a transient $\Delta R/R$ that matches the steady-state-derived analogue (Fig. S6). The low cross-plane thermal conductivity of 2DHPs yields a timescale of heat dissipation that is much longer than the plotted 100-ps window [35-37]. A complete establishment of late-time response takes slightly longer in n=2 (~70 ps) than in n=1 (~40 ps), likely arising from a larger inorganic-layer thickness over which the organic-to-inorganic vibrational energy transfer process takes place.

Focusing on the 78-K results hereafter, to interpret the early-time transient response we resort to the Lorentzian oscillator model by independently varying one of its four parameters starting from the experimentally fitted values for n=1 (Table S1). The calculated $\Delta R/R$ curves are shown in Fig. 3a (3b) when varying ω_{L} and γ (varying ε_{∞} and A_{L}). Fig. 3a suggests that an increase (or for a similar reason, a decrease) in ω_{L} does not reproduce the early-time response but yields a $\Delta R/R$ line-shape that resembles the late-time transient response. This is consistent with the steady-state exciton blueshift with increasing temperature, although in the steady-state case a temperature increase also leads to changes in ε_{∞}, A_{L} and γ (Table S1-S2). While increasing γ yields a $\Delta R/R$ line-shape similar to the early-time transient response, it predicts twice as large of an amplitude of

$\Delta R/R$ on the blue side as that on the red side, inconsistent with experiments. More reflectance calculations for both materials by sweeping the Lorentzian parameters yield similar $\Delta R/R$ spectral shapes (Fig. S7-S8).

Fig. 3b demonstrates that decreasing ε_∞ leads to a derivative line-shape with the sign of $\Delta R/R$ opposite to the experimental results, and a non-vanishing change in reflectance persisting into the high frequency range. Notably, a decrease in A_L (Fig. 3b) can reproduce the shape of $\Delta R/R$ and relative amplitudes on both sides of the zero-crossing wavelength. Therefore, we attribute the early-time response to a reduction in the exciton oscillator strength. In the simple Lorentzian picture describing non-interacting polarizable excitons, the oscillator strength scales as $A_\mathrm{L} = \frac{Ne^2}{\varepsilon_0 m}$, where e is the elementary charge, ε_0 is the vacuum permittivity, and N and m are the density and effective mass of the excitons, respectively. Since organic-to-inorganic vibrational energy transfer takes tens of ps, at early times (*e.g.*, 5 ps), the response is largely dominated by *intra*molecular vibrations of the BA^+ cations with the Pb-Br framework remaining unperturbed. As such, we expect the exciton effective mass m, which is dictated by the in-plane orbital overlap between the lead and bromide ions [7], to stay unchanged. Therefore, the early-time reduction in A_L is primarily attributable to a reduction in N that is understood as follows: vibrational excitation of the organic cations produces a transient strain and their thermal expansion, which then elongates the material along the out-of-plane direction and reduces the volumetric density of the Pb-Br octahedral layers in a macroscopic sense (*i.e.*, the number of Pb-Br layers per unit length is reduced despite the thickness of individual Pb-Br layer remaining unchanged). In turn, this leads to a reduction of the oscillator strength since the exciton-hosting Pb-Br layers per unit volume decreases. As delay time advances, organic-to-inorganic vibrational energy transfer leads to structural variations in the inorganic layer and the associated late-time transient response (Fig. 2). The transition from the first to the second temporal regime marks the fundamental timescales of vibrational energy dissipation from the organic to the inorganic spacer.

The above picture is validated by the stronger $\Delta R/R$ amplitude of n=1 in comparison to n=2, since the larger volumetric ratio of organic/inorganic constituents in n=1 compared to n=2 should produce a stronger amplitude of photoinduced strain. The observed timescale of transient expansion of the organic spacers is in concert with study on vibrationally-excited phospholipids using ultrafast electron diffraction [38]. A qualitative estimate on the photoinduced strain at early

times can be deduced, since A_L scales linearly with N, and inversely proportionally with unit-cell volume. Therefore, in the small perturbation regime, there is a one-to-one correspondence between the ΔA_L and Δc, as plotted in Fig. 3c, where Δc is the change in the lattice constant along c axis. For n=1, the relation between $\Delta R/R$ and ΔA_L obtained from transfer-matrix calculations (Fig. S7), in conjunction with the $\Delta R/R$ transient spectrum (Fig. 2b; $|\Delta R/R_{max}| \approx 2.3\%$ at 399 nm), allows an estimate on the pump-induced reduction in A_L to be about 3 meV. This corresponds to a Δc on the order of 0.04~0.05 Å and an estimated transient strain of 0.14~0.18%. This value slightly underestimates the true strain since the reduction in ε_∞ is not considered (contributed by bound electrons and hence roughly scales with material density), which should yield opposite changes in $\Delta R/R$ than that caused by a reduction in A_L. Furthermore, such a level of transient strain of the organic spacers is not expected to significantly impact ω_L, since it was shown that variation in ω_L is less than 20 meV even with an increase in the organic-spacer length up to 10 Å [20]. Quantitative information on the photoinduced strain could be further investigated by time-resolved X-ray diffraction [39,40].

Having established the MIR pump-induced transient organic sub-lattice expansion, we then investigate the impact of MIR excitation on the photoluminescence (PL) intensity and dynamics of n=1 at 78 K. In the so-called MIR-pump PL-probe experiments (see Methods) [41,42], the sample is excited by both the MIR pulse and an UV PL-excitation pulse at 370 nm. The time-integrated PL obtained at two different UV-pulse fluences, both with and without the MIR excitation, are presented in Fig. 4a, where the MIR pulse arrives 1-ps earlier than the UV pulse. Two prominent peaks can be identified with a 35-meV (62 meV) energy separation at low (high) fluence. The higher-energy peak centered at ~412 nm matches with that acquired using a ps laser with much lower fluence (Fig. S9) and is assigned to free-exciton emission. The lower-energy peak, absent under ps-laser excitation, can be ascribed to biexciton emission, since its energy separation from the exciton peak compares well with reported biexciton binding energy of 30~60 meV [43-45]. The PL intensities versus excitation fluence (Fig. 4b) reveal that at the low-to-intermediate fluence range (0~20 μJ·cm^{-2}, inset), the biexciton (exciton) intensity scales as $N^{1.35}$ ($N^{0.70}$), where N is the exciton density proportional to the fluence. Since we did not observe bleaching or degradation of the n=1 sample in the explored fluence range of the UV excitation pulse (Fig. S10-11), the sublinear growth of the exciton and biexciton intensities at high excitation fluence (>20 μJ·cm^{-2}) likely arises from exciton-exciton annihilation [46].

Interestingly, n=1 exhibits enhanced biexciton emission and suppressed free-exciton emission if pre-excited by the MIR pump. By tuning the relative temporal delay between the MIR and the UV pulses, we observe biexciton enhancement for n=1 over a range of delay times (Fig. S12) only when the MIR-pump arrives earlier than the UV pulse, hence we can exclude the optical Stark effect [47] to be responsible for biexciton enhancement. Furthermore, we can eliminate resonant high-harmonic generation [48] or multi-photon absorption [49], since no PL signal was observed with the MIR excitation alone (Table S1 caption). Fig. 4c displays the ratio of biexciton intensities with and without the MIR pump, and the same for the total PL intensity (*i.e.*, biexciton and exciton combined), obtained by fitting the free exciton and biexciton emission peaks using two Gaussians (Table S3). We find that at low-to-intermediate fluences, biexciton PL enhancement outweighs the suppression in free-exciton PL, and therefore the material overall becomes brighter under pre-excitation by MIR pulses.

It was shown that 2DHPs host stable biexcitons and even exhibit superfluorescence at room temperature, despite strong dynamic motions of the organic cations [50,51]. The formation of large polarons and screening by the dynamically disordered organic spacers were proposed as possible mechanisms to protect the charge carriers from scattering with defects and from exciton dephasing [51,52]. However, the observed *increase* in biexciton intensity under MIR vibrational excitation is unusual, since biexciton stability typically decreases with lattice temperature owing to thermally activated biexciton dissociation into two excitons [53]. The fact that biexciton emission increases despite enhanced vibrations of the organic cations validates that the inorganic lattice remains "cold" in the early stage. Since the exciton binding energy is larger than thermal energy at 78 K, once two excitons are combined to form a biexciton they are not influenced by the late-time transient lattice temperature rise. Here, we attribute the MIR pump-induced enhancement in biexciton intensity to diminished interlayer exciton tunneling. For 2DHPs, interlayer exciton tunneling has been directly observed by spatiotemporal PL imaging [19], and indirectly inferred from the threefold enhancement in charge-carrier mobility with 1% interlayer lattice contraction [54]. Double-quantum coherence spectroscopy [55], 2D electronic spectroscopy [56], and Fourier imaging [57] experiments showed evidence of interlayer exciton coupling. Here, the MIR pump lengthens organic spacers, reducing exciton wave-function overlaps between neighboring Pb-Br layers and suppressing interlayer exciton migration. This, in turn, increases intralayer carrier confinement and promotes exciton binding to form biexcitons. At high pump fluence, the effect of MIR excitation

becomes inconsequential due to strong exciton-exciton annihilation (*e.g.*, via significant Auger process).

Another contribution to the enhanced biexciton and overall PL intensity may arise from thermally activated detrapping of excitons. Fig. 4d presents the decay kinetics of free excitons obtained from streak-camera measurements (Fig. S13; integration from 408 to 415 nm). The fact that the free-exciton intensity scales sub-linearly with the fluence ($\propto N^{0.70}$) and the deviation of from a mono-exponential decay (Fig. 4d) suggest the presence of defect and trap states, effective in capturing charge carriers and suppressing radiative decay of excitons. The elongated exciton lifetimes induced by MIR excitation (Fig. 4d) suggest exciton detrapping from shallow traps and defect states (such as those attributed to organic cation vacancies), leading longer lifetimes and a higher density of excitons and biexcitons [58].

In summary, we showed that 2DHPs exhibit two different regimes of transient response following impulsive excitation of the organic vibrations using MIR pulses. The early-time transient response is associated with transient thermal expansion of the organic spacers, which leads to a reduction in the exciton oscillator strength. We identify several tens of ps as the characteristic timescale of organic-to-inorganic vibrational energy transfer, after which the Pb-Br sub-lattice reaches thermal equilibrium with the organic spacers. While our work shows MIR excitation strongly perturbs the organic spacers, a direct impact of MIR excitation on the octahedral layers may also be present and warrants further investigation by ultrafast electron diffraction [59] or time-resolved X-ray diffraction experiments [39]. In addition, we showed that MIR excitation of organic spacers can increase the biexciton and total PL quantum yield of n=1. Considering that biexcitons show a higher optical gain coefficient than free excitons, our experiments demonstrate that MIR vibrational excitation can serve as an effective external tuning knob to control exciton and biexciton strength in enhancing light-emitting [60,61,62] and lasing [63,64] characteristics, and in quantum optics applications for enhancing photon-pair generation [65]. Impulsive MIR excitation may be further conceived for manipulating magnetic dipole emission from 2DHPs or engineering exciton-polaritons to enable low-threshold lasers and novel quantum phases [66,67].

Acknowledgements

We acknowledge the support from the Air Force Office of Scientific Research (Grant No. FA9550-22-1-0209). C.C.S. acknowledges support from Special Account of Research Funding of the University of Crete (Grant No. KA 10652). Work at Northwestern University is supported by the Department of Energy, Office of Science, Basic Energy Sciences, under Grant No. SC0012541 (sample synthesis and characterization).

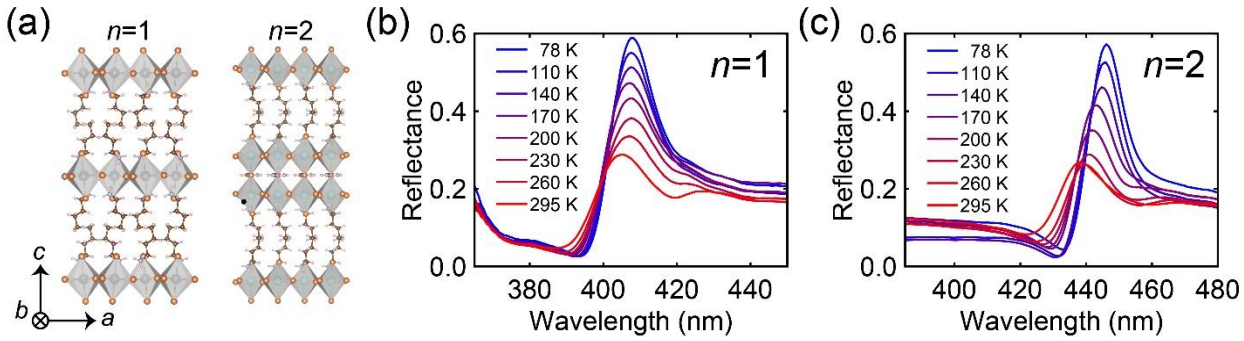

FIG. 1. (a) Crystal structures of the 2DHPs (left, n=1; right, n=2). Temperature-dependent, steady-state reflectance spectra for n=1 in (b) and n=2 in (c).

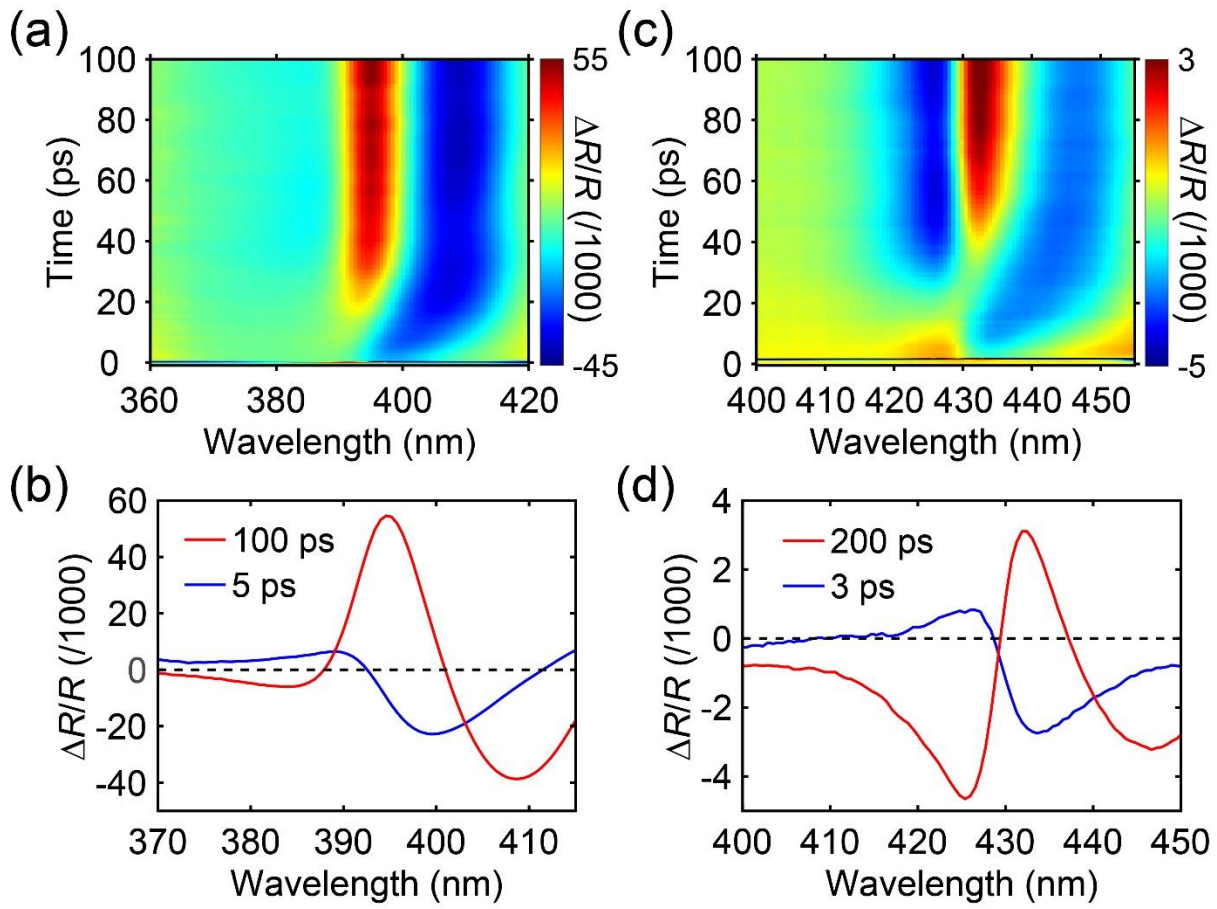

FIG. 2. Transient $\Delta R/R$ spectral map for n=1 in (a) and n=2 in (b) and $\Delta R/R$ spectra at selected delay times for n=1 in (b) and n=2 in (c). Measurements were performed at 78 K at fluence of 2.8 mJ·cm^{-2}.

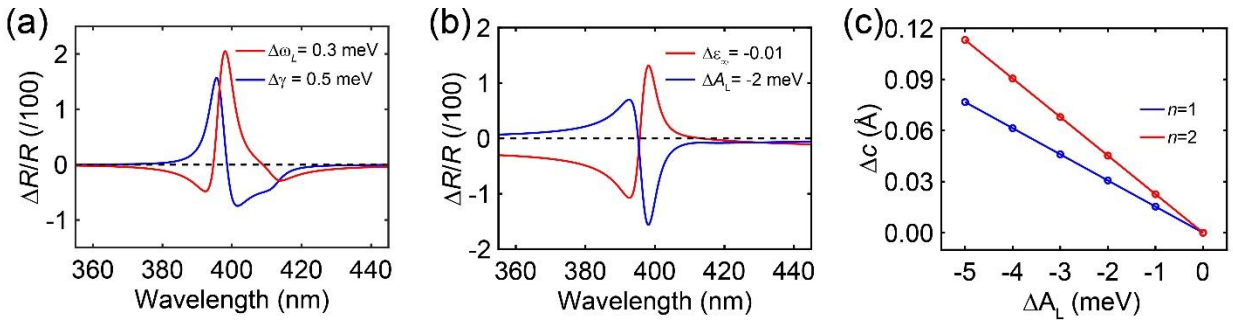

FIG. 3. Transfer-matrix calculated $\Delta R/R$ spectra by varying ω_{L} and γ in the Lorentzian model in (a) and by varying ε_{∞} and A_{L} in (b) . (c) Dependence of lattice constant along the *c* (out-of-plane) direction on the change in A_{L}.

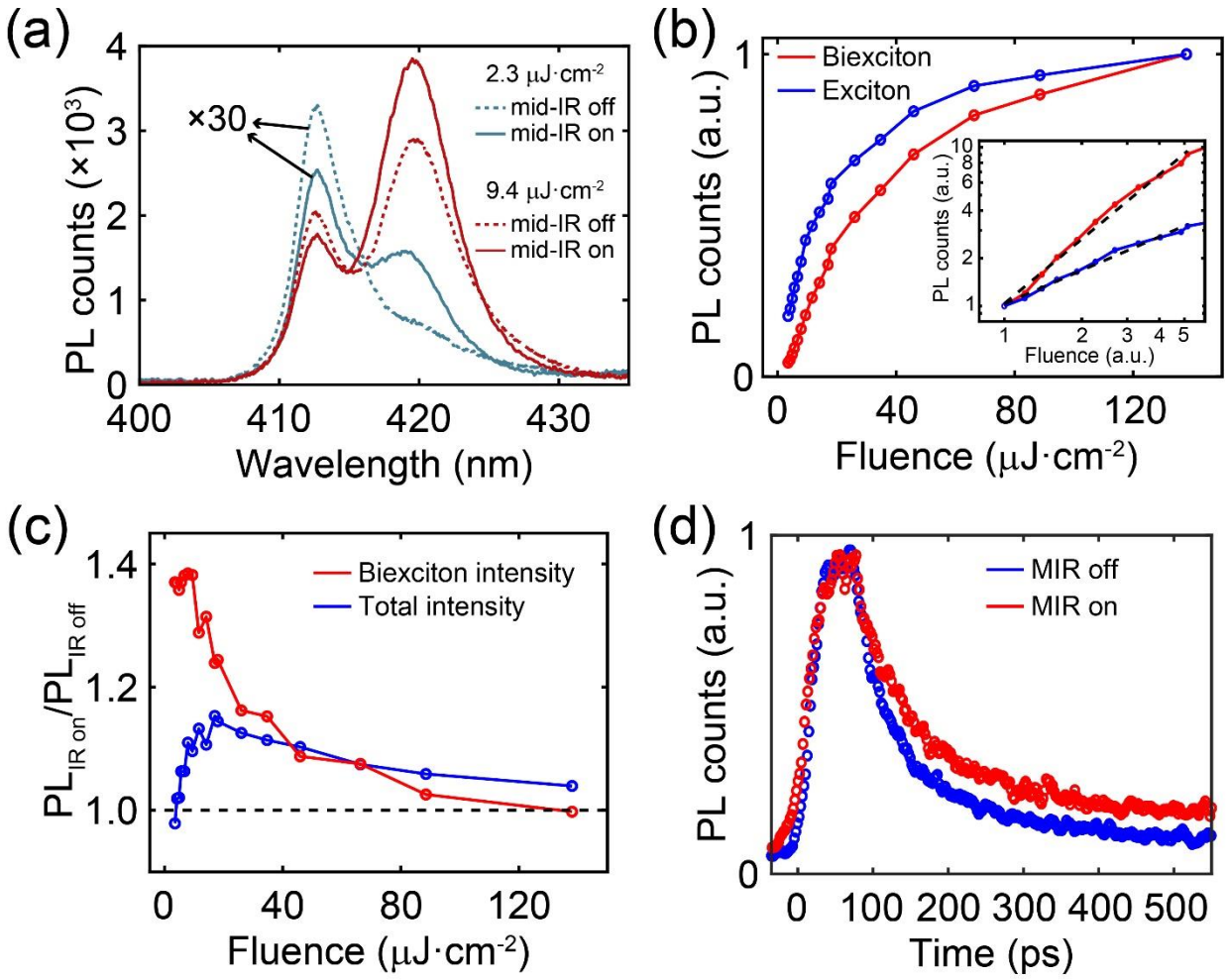

FIG. 4. (a) Time-integrated PL spectra for n=1 under two different excitation fluences (370-nm excitation), both with and without MIR pump with 13 mJ·cm^{-2} fluence. (b) Exciton and biexciton PL intensities vs. excitation fluence; inset shows logarithmic plot at low fluence range (0~20 μJ·cm^{-2}). (c) Ratios of emission intensities as a function of fluence of the UV pulse, obtained with and without the MIR pre-excitation; the total intensity includes both biexciton and free-exciton emission. The fluences in the inset of (a) and in the axis labels of (b) and (c) refer to the UV excitation pulse. (d) Time-resolved PL decays for free-exciton emission from n=1, with and without the MIR pump excitation (extracted from Fig. S13 by integrating the PL from 408 to 415 nm).

References

[1] L. Pedesseau *et al.*, ACS Nano **10**, 9776 (2016).
[2] M. M. Lee, J. Teuscher, T. Miyasaka, T. N. Murakami, and H. J. Snaith, Science **338**, 643 (2012).
[3] L. Mao, W. Ke, L. Pedesseau, Y. Wu, C. Katan, J. Even, M. R. Wasielewski, C. C. Stoumpos, and M. G. Kanatzidis, Journal of the American Chemical Society **140**, 3775 (2018).
[4] C. C. Stoumpos, D. H. Cao, D. J. Clark, J. Young, J. M. Rondinelli, J. I. Jang, J. T. Hupp, and M. G. Kanatzidis, Chemistry of Materials **28**, 2852 (2016).
[5] X. Li, J. M. Hoffman, and M. G. Kanatzidis, Chemical Reviews **121**, 2230 (2021).
[6] B. Saparov and D. B. Mitzi, Chemical Reviews **116**, 4558 (2016).
[7] C. Katan, N. Mercier, and J. Even, Chemical Reviews **119**, 3140 (2019).
[8] H. Tsai *et al.*, Nature **536**, 312 (2016).
[9] E. R. Dohner, A. Jaffe, L. R. Bradshaw, and H. I. Karunadasa, Journal of the American Chemical Society **136**, 13154 (2014).
[10] R. Su, A. Fieramosca, Q. Zhang, H. S. Nguyen, E. Deleporte, Z. Chen, D. Sanvitto, T. C. H. Liew, and Q. Xiong, Nature Materials **20**, 1315 (2021).
[11] C. Qin, A. S. D. Sandanayaka, C. Zhao, T. Matsushima, D. Zhang, T. Fujihara, and C. Adachi, Nature **585**, 53 (2020).
[12] L. Li *et al.*, Journal of the American Chemical Society **140**, 6806 (2018).
[13] E. Shi *et al.*, Nature **580**, 614 (2020).
[14] Y.-H. Kim *et al.*, Science **371**, 1129 (2021).
[15] B. Cai, X. Chen, M. Xie, S. Zhang, X. Liu, J. Yang, W. Zhou, S. Guo, and H. Zeng, Materials Horizons **5**, 961 (2018).
[16] G. Wang, A. Chernikov, M. M. Glazov, T. F. Heinz, X. Marie, T. Amand, and B. Urbaszek, Reviews of Modern Physics **90**, 021001 (2018).
[17] P. Guo *et al.*, Physical Review Letters **121**, 127401 (2018).
[18] O. Yaffe, A. Chernikov, Z. M. Norman, Y. Zhong, A. Velauthapillai, A. van der Zande, J. S. Owen, and T. F. Heinz, Physical Review B **92**, 045414 (2015).
[19] Z. Shi, Z. Ni, and J. Huang, ACS Energy Letters **7**, 984 (2022).
[20] T. Ishihara, J. Takahashi, and T. Goto, Physical Review B **42**, 11099 (1990).
[21] C. R. Kagan, D. B. Mitzi, and C. D. Dimitrakopoulos, Science **286**, 945 (1999).
[22] C. Li *et al.*, Nano Letters **21**, 3708 (2021).
[23] T. Neumann *et al.*, Nature Communications **12**, 3489 (2021).
[24] M. Menahem, Z. Dai, S. Aharon, R. Sharma, M. Asher, Y. Diskin-Posner, R. Korobko, A. M. Rappe, and O. Yaffe, ACS Nano **15**, 10153 (2021).
[25] E. S. Vasileiadou and M. G. Kanatzidis, Israel Journal of Chemistry **61**, 782 (2021).
[26] T. Sheikh and A. Nag, The Journal of Physical Chemistry C **123**, 9420 (2019).
[27] G. Scuri *et al.*, Physical Review Letters **120**, 037402 (2018).
[28] Y. Li *et al.*, Physical Review B **90**, 205422 (2014).
[29] B. Song *et al.*, ACS Materials Letters **3**, 148 (2021).
[30] J. C. Blancon *et al.*, Nature Communications **9**, 2254 (2018).
[31] D. B. Straus and C. R. Kagan, The Journal of Physical Chemistry Letters **9**, 1434 (2018).
[32] H. Mathieu, P. Lefebvre, and P. Christol, Physical Review B **46**, 4092 (1992).
[33] A. Raja *et al.*, Nature Communications **8**, 15251 (2017).
[34] M. A. Pérez-Osorio, R. L. Milot, M. R. Filip, J. B. Patel, L. M. Herz, M. B. Johnston, and F. Giustino, The Journal of Physical Chemistry C **119**, 25703 (2015).

[35] A. D. Christodoulides *et al.*, ACS Nano **15**, 4165 (2021).
[36] A. Giri, A. Z. Chen, A. Mattoni, K. Aryana, D. Zhang, X. Hu, S.-H. Lee, J. J. Choi, and P. E. Hopkins, Nano Letters **20**, 3331 (2020).
[37] P. Guo, C. C. Stoumpos, L. Mao, S. Sadasivam, J. B. Ketterson, P. Darancet, M. G. Kanatzidis, and R. D. Schaller, Nature Communications **9**, 2019 (2018).
[38] S. Chen, M. T. Seidel, and A. H. Zewail, Angewandte Chemie International Edition **45**, 5154 (2006).
[39] B. Guzelturk *et al.*, Nature Materials **20**, 618 (2021).
[40] E. M. Mannebach *et al.*, Nano Letters **17**, 7761 (2017).
[41] F. Sekiguchi, H. Hirori, G. Yumoto, A. Shimazaki, T. Nakamura, A. Wakamiya, and Y. Kanemitsu, Physical Review Letters **126**, 077401 (2021).
[42] P. Guo *et al.*, Nature Communications **10**, 482 (2019).
[43] Y. Cho, S. M. Greene, and T. C. Berkelbach, Physical Review Letters **126**, 216402 (2021).
[44] T. Ishihara, X. Hong, J. Ding, and A. V. Nurmikko, Surface Science **267**, 323 (1992).
[45] Y. Kato, D. Ichii, K. Ohashi, H. Kunugita, K. Ema, K. Tanaka, T. Takahashi, and T. Kondo, Solid State Communications **128**, 15 (2003).
[46] A. Srivastava and J. Kono, Physical Review B **79**, 205407 (2009).
[47] Y. Yang, M. Yang, K. Zhu, J. C. Johnson, J. J. Berry, J. van de Lagemaat, and M. C. Beard, Nature Communications **7**, 12613 (2016).
[48] L. Yao *et al.*, Journal of the American Chemical Society **143**, 16095 (2021).
[49] W. Chen, S. Bhaumik, S. A. Veldhuis, G. Xing, Q. Xu, M. Grätzel, S. Mhaisalkar, N. Mathews, and T. C. Sum, Nature Communications **8**, 15198 (2017).
[50] F. Thouin *et al.*, Physical Review Materials **2**, 034001 (2018).
[51] M. Biliroglu *et al.*, Nature Photonics **16**, 324 (2022).
[52] H. Zhu, K. Miyata, Y. Fu, J. Wang, P. P. Joshi, D. Niesner, K. W. Williams, S. Jin, and X.-Y. Zhu, Science **353**, 1409 (2016).
[53] Z. He *et al.*, ACS Nano **10**, 2176 (2016).
[54] W. Li *et al.*, Nature Nanotechnology **17**, 45 (2022).
[55] M. H. Elkins, R. Pensack, A. H. Proppe, O. Voznyy, L. N. Quan, S. O. Kelley, E. H. Sargent, and G. D. Scholes, The Journal of Physical Chemistry Letters **8**, 3895 (2017).
[56] A. H. Proppe *et al.*, The Journal of Physical Chemistry Letters **10**, 419 (2019).
[57] A. Fieramosca *et al.*, ACS Photonics **5**, 4179 (2018).
[58] Z. Ye *et al.*, Nature Communications **9**, 3718 (2018).
[59] H. Zhang *et al.*, arXiv:2204.01145 (2022)
[60] A. Fakharuddin *et al.*, Nature Electronics **5**, 203 (2022).
[61] V. I. Klimov, The Journal of Physical Chemistry B **110**, 16827 (2006).
[62] J. Shi *et al.*, Nature Nanotechnology **16**, 1355 (2021)
[63] T. Kondo, T. Azuma, T. Yuasa, and R. Ito, Solid State Communications **105**, 253 (1998).
[64] J. Q. Grim, S. Christodoulou, F. Di Stasio, R. Krahne, R. Cingolani, L. Manna, and I. Moreels, Nature Nanotechnology **9**, 891 (2014).
[65] R. M. Stevenson, R. J. Young, P. Atkinson, K. Cooper, D. A. Ritchie, and A. J. Shields, Nature **439**, 179 (2006).
[66] R. A. DeCrescent *et al.*, Science Advances **6**, eaay4900 (2020).
[67] S. B. Anantharaman *et al.*, Nano Letters **21**, 6245 (2021).